

# Mass conservation analysis of extrusion-based 3D printing simulations based on the level-set method

Carlos J.G. Rojas<sup>a,\*</sup>, C. A. Gómez-Pérez<sup>a</sup> and Leyla Özkan<sup>a</sup>

<sup>a</sup>Control Systems Group, Eindhoven University of Technology, Eindhoven, 5600MB, The Netherlands

## ARTICLE INFO

### Keywords:

Extrusion-based additive manufacturing  
Numerical simulation  
Level set method  
Mass conservation

## ABSTRACT

Numerical simulations of extrusion-based printing require tracking evolving material boundaries, a challenging task due to possible topological changes and mass conservation issues. Inaccurate conservation of mass can lead to a mismatch between the extruded and simulated shapes, and generally to unreliable predictions of the actual ink behavior. This work investigates the mass conservation properties of the conservative level-set method in extrusion-based 3D printing applications. We analyze the effects of the level set parameters on the accuracy of mass conservation using the cross-sectional area of the deposited strand. We compare the cross-sectional areas obtained in the simulation with the ideal areas obtained from a mass balance when the system reaches a steady-state condition. The numerical results indicate that reducing the reinitialization and the interface thickness parameters decreases the errors in the cross-sectional area obtained. However, the reductions in error tend to decline and could lead to excessive computational cost. Furthermore, we also found that the typical strong mesh requirements can be lessened by selecting an adequate interface thickness. Finally, we obtained the cross-sectional areas from simulations with different printing settings and found that they show good agreement with the simulated and experimental data published in previous work.

## 1. INTRODUCTION

Extrusion-based additive manufacturing (EB-AM) has gained widespread application due to its relative simplicity and material flexibility. This 3D printing process can accommodate various materials (e.g., food, ceramics, bioinks, or concrete) and geometric scales (from  $\mu\text{m}$  to  $\text{cm}$ ), offering versatility in high- and low-volume manufacturing applications Altıparmak, Yardley, Shi and Lin (2022). However, this versatility must be matched with a reliable and consistent process. This is particularly critical when working with materials where experimental iteration may be limited or expensive Naghieh and Chen (2021). To address these limitations, simulations can predict and optimize the behavior of the process, reducing the cost and variability of exclusive physical experiments. Consequently, numerical modeling and simulation of the process have become fundamental tools for understanding how machine settings and material properties affect a printed object Balta and Altıncaynak (2022).

A well-defined simulation should accurately represent the essential physical mechanisms of the printing process. This implies selecting the appropriate properties of the material, boundary conditions, and numerical methods. A commonly applied strategy for two-phase flow simulations is the one-fluid method Tryggvason (2011). This approach employs a single set of equations for the entire domain but requires the location of the phases to compute the necessary properties (e.g., density and viscosity) Tryggvason (2011). A consistent definition of the fluid interface is critical to enforce first principles, such as mass conservation, and handle discontinuities throughout the domain Mirjalili, Jain and Dodd (2017). For 3D printing simulations, the most prevalent interface-capturing methods in the literature are the volume of fluid (VOF) Spangenberg, Leal Da Silva, Comminal, Mollah, Andersen and Stang (2021); Mollah, Comminal, Serdeczny, Pedersen and Spangenberg (2021), the coupled level set with VOF (CLSVOF) Comminal, Serdeczny, Pedersen and Spangenberg (2018); Serdeczny, Comminal, Pedersen and Spangenberg (2019) and the conservative level set (CLS) Balta and Altıncaynak (2022); Bakrani Balani, Mokhtarian, Salmi and Coatanéa (2023). The VOF methods are based on sharp interface capturing, while the CLS considers a diffuse transition. Sharp capturing methods require a more complex numerical solution due to the jumps in the interface, but have good conservation properties. In contrast, the CLS approach is easier to implement, but can have issues with mass conservation Mirjalili et al. (2017).

\*

 c.j.gonzalez.rojas@tue.nl (C.J.G. Rojas); c.a.gomez.perez@tue.nl (C.A. Gómez-Pérez); l.ozkan@tue.nl (L. Özkan)  
ORCID(s):

This study is centered on the CLS method. The CLS approach was proposed to maintain the simplicity of the classical level set method while improving its conservation capabilities Olsson and Kreiss (2005). The authors proposed the use of a smooth level set function and a specific advection scheme to induce good conservation properties. However, a reinitialization step is necessary to maintain the thickness of the interface constant Olsson and Kreiss (2005). This reinitialization can affect the convergence of the solution Olsson, Kreiss and Zahedi (2007) and requires careful treatment to avoid numerical accumulation of errors in the case of complex flows or long simulations Desjardins, Moureau and Pitsch (2008); McCaslin and Desjardins (2014); Chiodi and Desjardins (2017). In Chiu and Lin (2011), a more computationally attractive CLS strategy was proposed. The advection and reinitialization steps were combined into a single equation, reducing the computational demand in the original CLS. Although skipping the additional step (i.e, reinitialization) is desired, this method requires simultaneous adjustment of the parameter controlling the interface thickness  $\epsilon$  and the amount of reinitialization induced  $\gamma$ .

In this work, we analyze the effects of the conservative level set parameters ( $\epsilon, \gamma$ ) on the enforcement of mass conservation. This is quantified through the cross-sectional area of the printed strand. Different criteria have been proposed to select CLS parameters based on the local speed of the interface and the size of the mesh Jain (2022); Chiu and Lin (2011); Mirjalili, Ivey and Mani (2020). However, these criteria have been proposed on the basis of specific numerical discretization and meshing conditions. In 3D printing simulations, it is important to correctly capture the shape of the strand to properly characterize the roughness of the surface and the bonding between adjacent layers Comminal et al. (2018). Although there have been some works where the areas of a strand have been studied and validated against experiments Comminal et al. (2018); Bakrani Balani et al. (2023), this is the first time a numerical study of mass conservation has been conducted for 3D printing simulations. The remainder of this paper is organized as follows. In section II, we present all the relevant details for the modeling and simulation. Section III describes the methodology of the parametric analysis and the convergence test. The effects of the level set parameters are discussed in Section IV. Finally, the conclusions of this work are given in Section V.

## 2. MODEL DESCRIPTION

### 2.1. Fluid Flow Governing Equations

The equations of fluid motion for the extrusion and deposition of material provide fundamental macroscopic variables such as velocity and pressure. Considering an isothermal and incompressible flow, the Navier-Stokes equations describe the transport of mass and momentum:

$$\nabla \cdot \mathbf{v} = 0 \quad (1)$$

$$\rho \left( \frac{\partial \mathbf{v}}{\partial t} + (\mathbf{v} \cdot \nabla) \mathbf{v} \right) = -\nabla \cdot (-p\mathbf{I} + \sigma) + \mathbf{F}_o \quad (2)$$

where  $\rho$  denotes density,  $\mathbf{v}$  velocity,  $p$  pressure,  $\sigma$  the stress tensor and  $\mathbf{F}_o$  the force contribution from gravity and (or) surface tension. A generalized stress tensor is defined as:

$$\sigma = 2\mu\mathbf{D} \quad (3)$$

$$\mathbf{D} = \left( \frac{\nabla \mathbf{v} + (\nabla \mathbf{v})^T}{2} \right) \quad (4)$$

here  $\mu$  is the viscosity and  $\mathbf{D}$  is the strain-rate tensor. The viscosity of the ink depends on various factors, such as the properties of the material and the processing conditions, and is characterized using rheological tests Wilms, Daffner, Kern, Gras, Schutyser and Kohlus (2021). A Newtonian constitutive model can be used when the main objective of the model is to predict the cross-sectional shape of the strand Serdeczny, Comminal, Pedersen and Spangenberg (2018b). However, more complex models could be employed to predict the printing force Serdeczny et al. (2018b) or to include the effects of thermal conditions on the process Bakrani Balani et al. (2023).

## 2.2. Conservative Level Set Method

To represent the laminar two-phase (air-ink) flow that takes place during the deposition, a scalar field  $\phi$  is introduced to model the interface between the two fluids as shown in Fig 1. For the level set method,  $\phi$  varies between 0 (blue-ink) and 1 (red-air) and is advected by the velocity (computed with (1) and (2)) as follows:

$$\frac{\partial \phi}{\partial t} + \nabla \cdot (\mathbf{v}\phi) = F \quad (5)$$

$$F = \gamma \nabla \cdot \left( \epsilon \nabla \phi - \phi(1 - \phi) \frac{\nabla \phi}{|\nabla \phi|} \right) \quad (6)$$

where  $\epsilon$  is a parameter controlling the interface thickness and  $\gamma$  is the reinitialization parameter Chiu and Lin (2011). The conservative level set method proposed in Olsson and Kreiss (2005) has a relatively simple structure and is especially suitable for simulations of incompressible flow, because Eq. 5 has the form of a conservative law. If ideal advection is considered, then  $F = 0$ . For some specific initial conditions of  $\phi$ , the analytical solution of Eq. 5 is equivalent if  $F = 0$  or if  $F$  is given by Eq. 6. However, as shown in Olsson et al. (2007), it is necessary to stabilize Eq. 5 because numerical perturbations are not damped and could create distorted shapes during the solution. The effect of perturbations on the solution can be studied by recasting the level-set evolution as the Burgers equation. In Olsson et al. (2007), it was found that the effect of numerical perturbations on the solution has a time scale  $t \sim \epsilon/\gamma$ . Based on this time scale, the criteria to select  $\epsilon$  and  $\gamma$  are normally supported by the assumption that if  $\epsilon/\gamma \ll 1$  then the perturbation effects would be significantly faster than the advection dynamics. In this work, we use the single-step CLS method, which does not require a separate reinitialization step Chiu and Lin (2011). If Eq. 5 is solved using conservative numerical schemes and the level set parameters  $\epsilon$  and  $\gamma$  are properly tuned, then the mass of the fluids should be conserved.

There are some empirical recommendations on how to tune the level-set parameters. The thickness of the interface  $\epsilon$  is normally selected around the maximum element size of the mesh Olsson et al. (2007); Chiu and Lin (2011). Regarding the reinitialization parameter, the recommendations in Olsson et al. (2007) are to use  $\gamma = 1$  for constant velocities (for a small  $\epsilon$ ) or, based on the velocity gradient, to make  $\gamma$  equal to the magnitude of the maximum velocity ( $v_{max}$ ). Furthermore, for specific numerical methods and mesh definitions,  $\phi$  is bounded for  $\gamma > v_{max}$  and  $\epsilon > 0.5\Delta x$ , where  $x$  is the cell size of the mesh Jain (2022). Similarly, in Mirjalili et al. (2020), the authors found that, rather than using independent specific values, there should be a balance between  $\epsilon$  and  $\gamma$ .

## 2.3. Boundary and Coupling Conditions

The boundary conditions of the model are the no-slip condition on the nozzle walls, symmetry around the  $xz$  plane, an inlet flow rate on the top of the cylinder, the sliding wall at the bottom of the rectangular block, and open boundaries for the rest of the walls. From an operational perspective, two boundary conditions deserve more attention because they incorporate the manipulated variables of the process as follows:

$$V_{pl} = - \int_{\partial\Omega_{inl}} \mathbf{v} \cdot \mathbf{n} dS, \quad (7)$$

$$\mathbf{v}_{\partial\Omega_{bn}} = \mathbf{v}_{bn} \quad \mathbf{v}_{bn} = (\bar{v}_x, 0, 0) \quad (8)$$

In Eq 7, the normal contributions of  $\mathbf{v}$  over the boundary  $\partial\Omega_{inl}$  are given by the flow rate  $V_{pl}$ , and in Eq 8, the velocity on the boundary  $\partial\Omega_{bn}$  is set to  $\bar{v}_x$ , the relative nozzle speed. In terms of control,  $\bar{v}_x$  can be directly adjusted using the G code, but  $V_{pl}$  is implicitly related to the dynamics of the extrusion system.

The fluid flow and the level-set equations are coupled through the advection velocity, but also through the properties of the phases. The density and viscosity used in the fluid flow equations are defined based on a smooth transition given by the following expressions:

$$\rho = \rho_1 + (\rho_2 - \rho_1)H(\phi) \quad (9)$$

$$\mu = \mu_1 + (\mu_2 - \mu_1)H(\phi) \quad (10)$$

where  $H$  is a smooth Heaviside function Olsson et al. (2007); Chiu and Lin (2011).

**Table 1**  
Simulation Parameters

Parameter	Nomenclature	Values	Units
$D$	Nozzle Diameter	0.4	mm
$L$	Nozzle Length	2	mm
$\Delta Z$	Nozzle to bed distance	{0.24, 0.32, 0.4}	mm
$B_w$	Block width	1.2	mm
$B_h$	Block height	0.6	mm
$B_l$	Block Length	6	mm
$v_p$	Plunger speed	20	mm/s
$V_{pl}$	Inlet flow	1.257	mm <sup>3</sup> /s
$\bar{v}_x$	Nozzle speed	{10, 15, 20}	mm/s
$\rho$	Density of the material	1.0	g/cm <sup>3</sup>
$\mu$	Viscosity of the material	1000	Pa·s
$g$	gravity acceleration	-9.81	m/s <sup>2</sup>

## 2.4. Simulation Settings

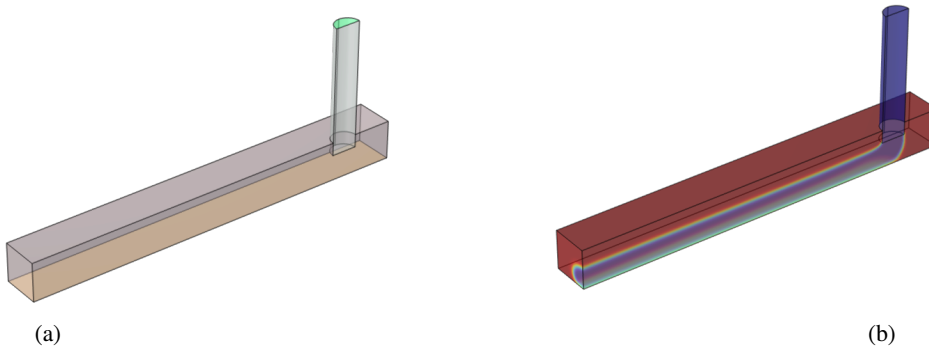


**Figure 1:** (a) Simulation domain. (b) Volume fraction of fluid (blue-ink, red-air)

The simulation is implemented in COMSOL Multiphysics® v6.2 COMSOL (2024), using the Laminar Flow and Level Set interfaces coupled with the Two-Phase Flow Level Set multiphysics. A stationary study step is defined to have a consistent initialization of the time-dependent solution, and the boundary conditions are ramped up to avoid numerical issues. The domain is defined according to the work in Serdeczny, Comminal, Pedersen and Spangenberg (2018a). The extrusion nozzle is modeled as a cylinder with diameter  $D$  and length  $L$ , and the distance between the tip of the nozzle and the bed is  $\Delta Z$ . The deposition domain is represented by a rectangular block, with cross-sectional dimensions  $B_w \times B_h$  and length  $B_l$ . A three-dimensional representation of the nozzle considering the  $xz$  symmetry of the domain is depicted in Fig 1. The effects of gravity are considered in the simulations and, for simplicity, the material is represented by a Newtonian constitutive model with viscosity  $\mu$ . All properties and dimensions used in the simulation are given in Table 1.

## 3. METHODOLOGY

### 3.1. Effects of level set parameters in 3D printing simulations

In a 3D printing study, ink deposition is characterized by a velocity that changes from the bottom of the bed to the top interface between ink and air. In addition, at the beginning of the simulation, it takes some time for the fluid to be deposited on the bed, and the use of a fixed reinitialization can create some mass conservation errors due to the proximity of the active (moving) and inactive (stationary) interfaces McCaslin and Desjardins (2014). Based on these conditions and the insights provided in the previous section, we analyzed how mass conservation is affected by the

level-set parameters. To avoid issues originating from the interaction of the active and inactive interfaces, we computed the cross sections of the strand 2 mm away from the nozzle axis at  $t = 0.5$  s.

### 3.1.1. Mass conservation analysis

Due to the high viscosity effects and the negligible influence of the inertial forces, a printed strand quickly reaches a steady state. Therefore, applying mass conservation (on a suitable control volume) and assuming a constant density, the following relationship holds:

$$V_{pl} = A\bar{v}_x \quad (11)$$

where  $A_f$  is the area of the strand. In addition, the inlet flow rate  $V_{pl}$  can be directly related to the cross-sectional area of the nozzle  $\pi D^2/4$  and the speed of the plunger  $v_p$ , which are the actual parameters of the process. We considered  $\Delta Z = 0.32$  mm and  $\bar{v}_x = 20$  mm/s to investigate the effects of the level set parameters. In Comminal et al. (2018); Serdeczny et al. (2018a), the authors compared the compactness of the strands obtained in the simulation with idealized cross sections. In contrast, we directly compared the area  $A_f$  calculated from the mass conservation in Eq. 11 to the following surface area:

$$A_s = \int_{\Omega} \xi(\phi) dA \quad (12)$$

$$\xi(\phi) = \begin{cases} 1, & \text{if } \phi \leq 0.5 \\ 0, & \text{otherwise} \end{cases} \quad (13)$$

for the different parameters of the level set method considered in this study. For  $\epsilon$ , we evaluated how the change in thickness around the maximum element size  $m_{max}$  affects the cross-sectional area of the fluid. In the case of  $\gamma$ , we proposed to use values around the nozzle printing speed  $\bar{v}_x$ , as this captures the most critical speed change.

### 3.1.2. Mass conservation analysis for different printing conditions

Once the effects of the level-set parameter have been established, we simulated the printing process for different settings. All simulations considered for this analysis used the best combination of  $\epsilon$  and  $\gamma$  found in the parametric study. We defined the same changes ( $\Delta Z$ ) and nozzle speeds ( $\bar{v}_x$ ) proposed in Serdeczny et al. (2018a) to validate the results with their simulated and experimental data.

## 3.2. Mesh convergence analysis

We performed a simple mesh refinement study to test the convergence of the solution for the settings  $\Delta Z = 0.32$  mm and  $\bar{v}_x = 20$  mm/s. The variables used to evaluate the convergence of the simulations were the surface area  $A_s$  and the maximum pressure on the nozzle  $P_{max}$ . With these two variables, we account for the effects of the mesh on both the fluid dynamics and the level-set solutions. For the level set solution, we used as a reference the strand area  $A_f$  explained in the previous subsection. Since the mesh size affects  $\epsilon$ , we also considered the difference between  $A_s$  and  $A_f$ :

$$\Delta A = \frac{|A_s - A_f|}{A_f} \times 100, \quad (14)$$

to select a single mesh for the mass conservation study. As a reference for the pressure, we considered the analytical Hagen-Poiseuille equation:

$$\Delta P = \frac{8\mu LV_{pl}}{\pi R^4}. \quad (15)$$

A mesh calibrated for fluid dynamics was created, and the element growth rate (1.08), curve factor (0.3), and resolution of narrow regions (0.95) were fixed. Only the maximum and minimum element sizes were refined during the convergence analysis.

**Table 2**  
Mesh comparison

	Number of elements	$A_s \times 1000 [mm^2]$		$P_{max} [MPa]$	
		$\gamma = 0.02$	$\gamma = 1$	$\gamma = 0.02$	$\gamma = 1$
<b>Mesh 1</b>	2077795	59.65	40.22	8.393	8.263
<b>Mesh 2</b>	3315894	61.58	51.45	8.381	8.323
<b>Mesh 3</b>	4957174	62.36	56.22	8.377	8.347

**Table 3**  
Effects of  $\gamma$  on the strand cross-section

$\gamma [m/s]$	$A_s \times 1000 [mm^2]$	$\Delta A\%$
0.005	60.34	3.96
0.01	60.11	4.33
<b>0.02</b>	<b>59.65</b>	<b>5.07</b>
0.04	58.74	6.52
0.08	57.06	9.19

## 4. RESULTS

All simulations performed in this work were implemented in the HPC cluster of the Eindhoven University of Technology. The jobs run on only one node with one task and 32 CPUs per task.

### 4.1. Mesh convergence results

The mesh convergence results are presented in Table II. As a starting point for this analysis, we considered the recommended  $\epsilon$  in COMSOL:

$$\epsilon_{ref} = \begin{cases} m_{max}, & \text{if } m_{max} > 1.3 * m_{min} \\ 2 * m_{max}, & \text{otherwise} \end{cases} \quad (16)$$

where  $m_{max}$  and  $m_{min}$  are the maximum and minimum element size around the fluid's interface. We used  $\gamma = \{0.02, 1\} m/s$ , the first value is based on the nozzle speed defined for this study, and the second is the default value for the reinitialization parameter in COMSOL. The maximum pressure in the domain  $P_{max}$  converged faster than  $A_s$ , which required a finer mesh to reach a relatively convergent value. Although  $A_s$  was still changing, we did not refine it further because the value obtained for mesh 3 is almost the same as the analytical value  $A_f$  with less than 1% error. Similarly,  $P_{max}$  was less than 5% higher than the reference  $\Delta P$ . The effects of  $\gamma$  are discussed in the following subsection; however, we already notice a big difference between  $A_s$  and the reference area  $A_f = 62.83e - 3 [mm^2]$  (for  $\bar{v}_x = 20 mm/s$ ) depending on the value of  $\gamma$ . Based on the computational time required for  $\gamma = 0.02$ , we decided to use mesh 1 because it took less simulation time compared to mesh 3 and still gave an acceptable error of around 5% in  $A_s$ .

### 4.2. Effects of the reinitialization parameter

We simulated the process for different values of the reinitialization parameter ( $\gamma$ ) to evaluate its effects on mass conservation. In Fig. 2, we see that the strand cross-section has an ellipsoidal shape and when  $\gamma$  increases, the major axis shrinks, while the minor axis expands. The surface areas ( $A_s$ ) obtained in the simulation for  $\gamma$  values around the nozzle speed  $\gamma_{ref} = 0.02$  are shown in Table III. Decreasing  $\gamma$  to 0.005 produced a slight improvement from around 5 to 4% error. In contrast, increasing  $\gamma$  had a greater impact on the precision of the results, as can be seen in the errors ( $\Delta A$ ) of the last two parameters in Table III. The simulation time was almost the same for the first two parameters compared to  $\gamma_{ref}$ . Furthermore, it was also noticed that for the last two parameters considered, there is a significant increase in the computation time.

### 4.3. Effects of the interface thickness

Since the default interface thickness used in COMSOL considers the maximum element size, we analyzed the effects of reducing its value. The default interface thickness for mesh 1 was  $\epsilon_{ref} = 0.043 [mm]$ , which is approximately

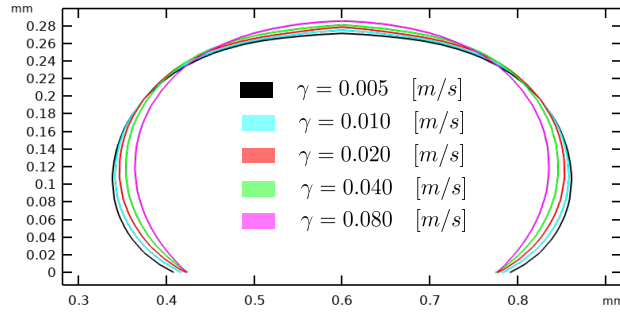


Figure 2: Effects of  $\gamma$  on cross-sections

Table 4

Effects of  $\epsilon$  on the strand cross-section

$\epsilon_f$ [-]	$A_s \times 1000$ [ $mm^2$ ]	$\Delta A\%$
<b>1.0</b>	<b>59.65</b>	<b>5.07</b>
0.9	60.89	3.10
0.8	61.77	1.69
0.7	62.67	0.68
0.6	63.26	0.25
0.5	63.74	1.44

7 times less than the nozzle-to-bed distance defined ( $\Delta Z = 0.32$  [mm]). For this analysis, we considered changes based on the factor  $\epsilon_f = \epsilon/\epsilon_{ref}$ . Decreasing  $\epsilon_f$  reduced the mass conservation error, as shown in Table IV. The parameters  $\epsilon_f = \{0.9, 0.8\}$  approximately halve the error, and the following two parameters  $\epsilon_f = \{0.7, 0.6\}$  give an error below 1%. Another interesting aspect of the results was that  $A_s$  starts to exceed the reference value  $A_f$  for the last two parameters, and there was an increase in the error when reducing  $\epsilon_f$  from 0.6 to 0.5. The qualitative effects of  $\epsilon$  on the cross-section are given in Fig. 3. Reducing the factor  $\epsilon_f$  lead to ellipsoids with a larger major axis; however, the changes in the minor axis did not seem significant. Regarding the computational cost, most parameters resulted in a similar simulation time, except for the last, which took slightly longer than the others.

Based on the effects of the interface thickness and the influence of the mesh size on  $A_s$ , we also performed an additional test in which we decreased the mesh refinement and found a  $\epsilon_f$  resulting in a small mass conservation error. The results of using a coarser mesh with  $\epsilon_{ref} = 0.069$  [mm] for different factors  $\epsilon_f$  are given in Table V. We observed a significant decrease in the cross-sectional error  $\Delta A$  from 14 to 0.2%. The interface thickness for the best result obtained

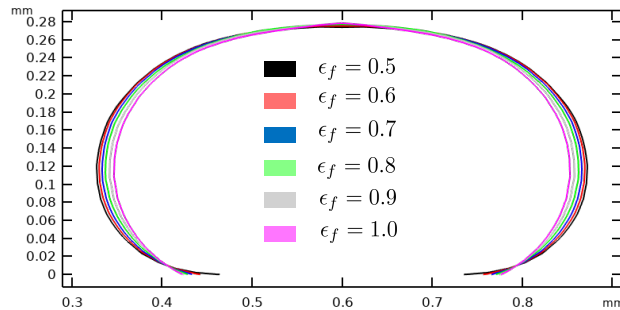


Figure 3: Effects of  $\epsilon$  on cross-sections

in Table IV is  $\epsilon_4 = 0.0258$  [mm], and the best result shown in Table V corresponds to  $\epsilon_5 = 0.0276$  [mm]. So, what seems to be important is to have an adequate interface thickness around the fluid interface. In terms of the qualitative effects on the cross-section, we compared the two results in Fig. 4. We see that there are some slight differences in the ellipsoids,

**Table 5** $\epsilon$  refinement for a coarser mesh

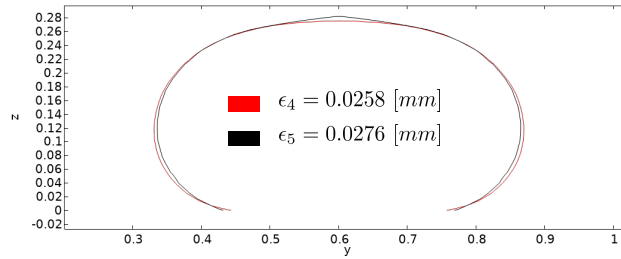
$\epsilon_f$ [-]	$A_s \times 1000$ [mm <sup>2</sup> ]	$\Delta A\%$
0.8	53.65	14.61
0.7	56.97	9.33
0.6	59.57	5.19
0.5	61.43	2.23
0.4	62.68	0.24
0.3	63.52	1.10

**Table 6**

Results for different printing parameters

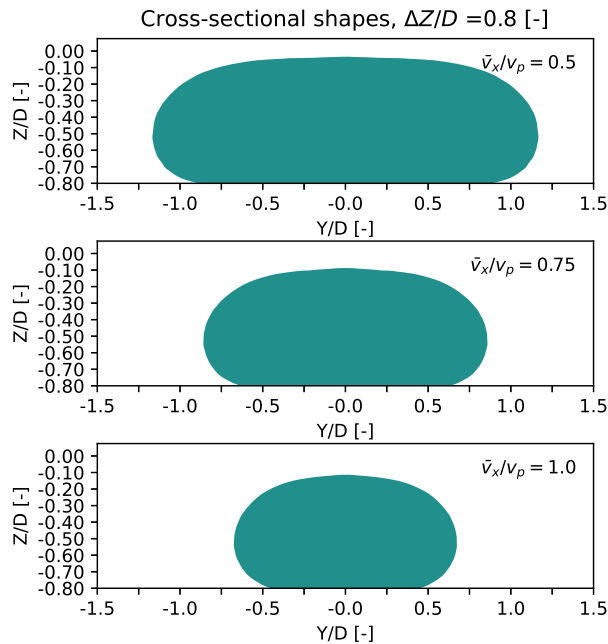
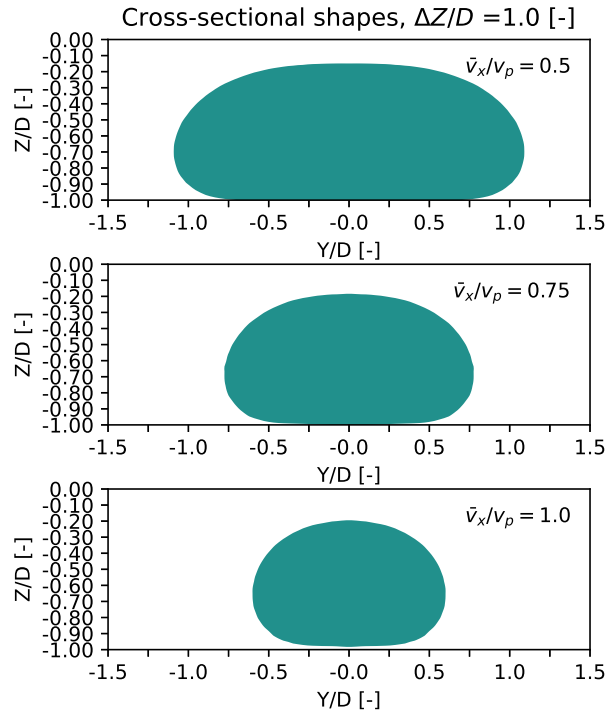
$\Delta Z/D$ [-]	$\bar{v}_x/v_p$ [-]	$A_s \times 1000$ [mm <sup>2</sup> ]	$\Delta A\%$
0.6	0.5	123.71	0.48
0.6	0.75	83.70	0.09
0.6	1.0	62.53	1.55
0.8	0.5	126.21	0.14
0.8	0.75	84.36	0.70
0.8	1.0	62.92	0.44
1.0	0.5	127.85	0.88
1.0	0.75	84.88	1.32
1.0	1.0	62.28	1.74

especially towards the top-centered part of the material. Finally, in terms of computational time, the simulation with  $\epsilon_4$  took around 6h while the one with  $\epsilon_5$  took around 3h.

**Figure 4:** Qualitative differences between  $\epsilon_4$  and  $\epsilon_5$ 

#### 4.4. Mass conservation analysis for different conditions

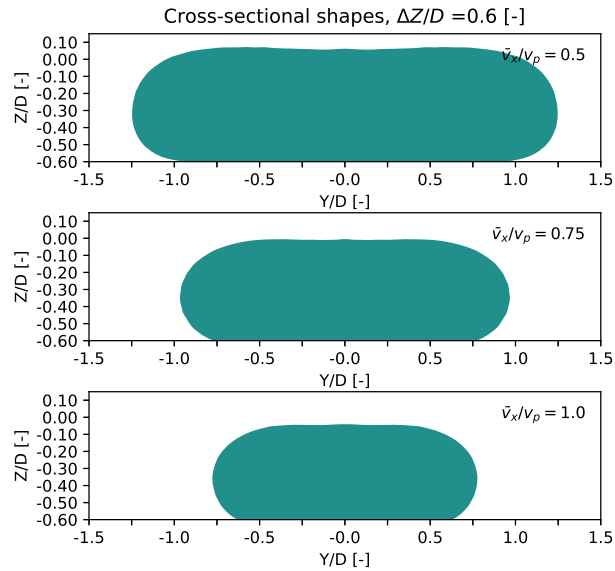
To conclude with the numerical analysis, we used the best level set parameters found in the previous subsections ( $\gamma = 0.005$  m/s,  $\epsilon = 0.0276$  mm) to evaluate the precision of the simulations for different nozzle-to-bed distances ( $\Delta Z$ ) and nozzle speeds ( $\bar{v}_x$ ). The reference areas were scaled according to the ratio  $\bar{v}_x/v_p$  and the results are summarized in Table VI. We see that independently of the printing parameters, the errors are very small. In Figures 5 to 7, we present the cross-sectional areas obtained for these simulations. Although the reference areas  $A_f$  did not change with  $\Delta Z/D$ , the major axis of the strand shrank when the nozzle-to-bed distance was increased. We also observed that the qualitative behavior of the results was good compared to the experimental results given in Serdeczny et al. (2018a). In Table VII, we present the aspect ratio  $W/H$  obtained in this work and the values reported in Serdeczny et al. (2018a). There is a good agreement between the simulated (Sim) and experimental (Exp) data in Serdeczny et al. (2018a) and the results obtained in this work for almost all the conditions evaluated. Furthermore, the shapes of the areas seem to match the experimental results more accurately than the areas simulated in Serdeczny et al. (2018a).



**Table 7**

Aspect ratio comparison with reference

$\Delta Z/D$ [-]	$\bar{v}_x/v_p$ [-]	$W/H$	$W/H - Sim$	$W/H - Exp$
0.6	0.5	3.7	4.5	4.0
0.6	0.75	3.3	3.2	4.0
0.6	1.0	2.8	3.0	3.8
0.8	0.5	3.0	3.0	3.1
0.8	0.75	2.4	2.4	2.9
0.8	1.0	2.0	2.0	2.1
1.0	0.5	2.6	2.6	2.5
1.0	0.75	1.9	1.8	2.1
1.0	1.0	1.5	1.5	1.8

**Figure 7:** Cross-sectional shapes -  $\Delta Z/D = 0.6$ 

## 5. CONCLUSIONS

We proposed the first mass conservation study for 3D printing simulations based on the conservative level set method. There is no clear guide on how to tune the level-set parameters, and their effects on the cross-sectional area of a printed strand have not been quantified before. The numerical results indicate that by carefully reducing the reinitialization parameter and the interface thickness, the errors on the cross-sectional area are reduced. This indicates a better enforcement of mass conservation in the simulation. Although decreasing the level-set parameters seems logical, we found that the reductions in error tend to decrease at some point, and that excessive reduction can lead to higher computational cost. Furthermore, we also found that the requirements on mesh refinements that are common for the level-set method can be attenuated by selecting an adequate interface thickness. Normally, the recommendation in commercial software is to tune the reinitialization parameter, but the results show that careful refinement of the interface thickness can have a more significant impact on the mass conservation without compromising the computational cost. Finally, the best level set parameters found were used to simulate 3D printing scenarios with different settings. The quantitative results had small errors, and the cross-sectional shapes agree well with the experimentally validated results in the literature.

## 6. ACKNOWLEDGMENTS

The authors would like to thank Tusher Mollah and Monica Zakhari for the valuable discussions about the simulation settings and initial results. Furthermore, the authors would like to acknowledge the financial support from NWO (grant number: 18763), Wageningen Food & Biobased Research, TNO, Ruitenber Ingredients B.V., LambWeston Holdings, Inc., and Gastronomy 3D Food Works.

## CRedit authorship contribution statement

**Carlos J.G. Rojas:** Writing – review & editing, Writing – original draft, Visualization, Software, Methodology, Investigation, Conceptualization. **C. A. Gómez-Pérez:** Writing – review & editing, Conceptualization. **Leyla Özkan:** Writing – review & editing, Conceptualization, Supervision.

## References

- Altıparmak, S.C., Yardley, V.A., Shi, Z., Lin, J., 2022. Extrusion-based additive manufacturing technologies: State of the art and future perspectives. *Journal of Manufacturing Processes* 83, 607–636.
- Bakrani Balani, S., Mokhtarian, H., Salmi, T., Coatanéa, E., 2023. An Investigation of the Influence of Viscosity and Printing Parameters on the Extrudate Geometry in the Material Extrusion Process. *Polymers* 15, 2202.
- Balta, E.C., Altunkaynak, A., 2022. Numerical and experimental analysis of bead cross-sectional geometry in fused filament fabrication. *Rapid Prototyping Journal* 28, 1882–1894.
- Chiodi, R., Desjardins, O., 2017. A reformulation of the conservative level set reinitialization equation for accurate and robust simulation of complex multiphase flows. *Journal of Computational Physics* 343, 186–200.
- Chiu, P.H., Lin, Y.T., 2011. A conservative phase field method for solving incompressible two-phase flows. *Journal of Computational Physics* 230, 185–204.
- Comminal, R., Serdeczny, M.P., Pedersen, D.B., Spangenberg, J., 2018. Numerical modeling of the strand deposition flow in extrusion-based additive manufacturing. *Additive Manufacturing* 20, 68–76.
- COMSOL, I., 2024. Comsol multiphysics reference manual, version 6.3. [www.comsol.com](http://www.comsol.com).
- Desjardins, O., Moureau, V., Pitsch, H., 2008. An accurate conservative level set/ghost fluid method for simulating turbulent atomization. *Journal of Computational Physics* 227, 8395–8416.
- Jain, S.S., 2022. Accurate Conservative Phase-Field Method for Simulation of Two-Phase Flows. SSRN Electronic Journal .
- McCaslin, J.O., Desjardins, O., 2014. A localized re-initialization equation for the conservative level set method. *Journal of Computational Physics* 262, 408–426.
- Mirjalili, S., Ivey, C.B., Mani, A., 2020. A conservative diffuse interface method for two-phase flows with provable boundedness properties. *Journal of Computational Physics* 401, 109006.
- Mirjalili, S., Jain, S.S., Dodd, M., 2017. Interface-capturing methods for two-phase flows: An overview and recent developments. *Center for Turbulence Research Annual Research Briefs* 2017, 117–135.
- Mollah, M.T., Comminal, R., Serdeczny, M.P., Pedersen, D.B., Spangenberg, J., 2021. Stability and deformations of deposited layers in material extrusion additive manufacturing. *Additive Manufacturing* 46, 102193.
- Naghieh, S., Chen, X., 2021. Printability—A key issue in extrusion-based bioprinting. *Journal of Pharmaceutical Analysis* 11, 564–579.
- Olsson, E., Kreiss, G., 2005. A conservative level set method for two phase flow. *Journal of Computational Physics* 210, 225–246.
- Olsson, E., Kreiss, G., Zahedi, S., 2007. A conservative level set method for two phase flow II. *Journal of Computational Physics* 225, 785–807.
- Serdeczny, M.P., Comminal, R., Pedersen, D.B., Spangenberg, J., 2018a. Experimental validation of a numerical model for the strand shape in material extrusion additive manufacturing. *Additive Manufacturing* 24, 145–153.
- Serdeczny, M.P., Comminal, R., Pedersen, D.B., Spangenberg, J., 2018b. Numerical study of the impact of shear thinning behavior on the strand deposition flow in the extrusion-based additive manufacturing, in: Billington, D., Leach, R.K., Phillips, D., Riemer, O., Savio, E. (Eds.), *Proceedings of the 18th International Conference of the European Society for Precision Engineering and Nanotechnology*, pp. 283–284.
- Serdeczny, M.P., Comminal, R., Pedersen, D.B., Spangenberg, J., 2019. Numerical simulations of the mesostructure formation in material extrusion additive manufacturing. *Additive Manufacturing* 28, 419–429.
- Spangenberg, J., Leal Da Silva, W.R., Comminal, R., Mollah, M.T., Andersen, T.J., Stang, H., 2021. Numerical simulation of multi-layer 3D concrete printing. *RILEM Technical Letters* 6, 119–123.
- Tryggvason, G., 2011. *Direct Numerical Simulations of Gas–Liquid Multiphase Flows*. Cambridge University Press, Cambridge.
- Wilms, P., Daffner, K., Kern, C., Gras, S., Schutyser, M., Kohlus, R., 2021. Formulation engineering of food systems for 3D-printing applications – A review. *Food Research International* 148, 110585.